Chapter 4

Electrocatalytic Properties of Gold on Gold, Platinum, and Graphite Surfaces for Alcohol Oxidation Reactions in Alkaline Medium

In this chapter, we discuss the electro-oxidation of alcohols such as methanol and ethanol on mesoporous gold deposited on gold (Au/Au), platinum (Au/Pt) and graphite (Au/C) substrates in an alkaline medium. In chapter 3, we have shown that high surface area mesoporous gold can be grown on gold surface electrochemically. Here, we show that the gold can also be deposited on platinum, and graphite surfaces using the similar procedure. The gold deposition was carried out by anodic dissolution of gold wire in equimolar mixture of ethanol solution of 11-mercaptoundecanoic acid (MUA) and aqueous solution of KCl. The real electroactive surface of the deposited film on these substrates were determined using stripping voltammetry in acid medium. Electrochemically grown gold on platinum, and graphite surfaces show the typical gold oxide stripping peaks. The surface characterization was carried out using scanning electron microscopy (SEM), and grazing angle X-ray diffraction (XRD). The SEM images show the porous structure of deposited gold. XRD shows the broadening of the peaks, indicating the deposited gold particles are nanometer size. We have studied the electro-oxidation of mesoporous gold on gold, platinum, and graphite in alkaline medium using cyclic voltammetry and chronoamperometry at different temperatures. From the CV data at different temperatures the activation energies (E_a) was measured. The chronoamperometry (CA) studies were carried out with and without prior potential programming at different potentials and temperatures to calculate the Tafel slope.

4.1 Introduction

The studies on electrocatalytic oxidation of alcohols using precious metal catalysts have attracted considerable interest in recent times [1-4]. Pt-based metal or alloy nanoparticles are of great deal of research interest in a number of areas [5]. Precious metal platinum is known to be a good catalyst for electro-oxidation of methanol in direct methanol fuel cells (DMFC) [6-9]. However, DMFCs are still limited by high production costs due to reliance on Pt and its alloy materials. One major effort is on enhancing Pt utilization through modifying the surfaces of non-Pt nanoparticles [10-12]. The Pt utilization in catalysts can be defined as the dispersion or exposed percentage of Pt atoms in the catalyst [10].

The direct electro-oxidation of methanol on Pt is complicated because of generation of strongly adsorbed intermediates, which are formed during the electro-oxidation of methanol [13-16]. On the other hand the catalytic property of gold is one of the fastest growing research topics in the field of catalysis. Exploration of gold nanoparticles in catalysis has attracted a wide range of fundamental and industrial interests. Au is generally considered as an inert material, but recent studies discovered that Au could exhibit a series of unusual properties when size decreases down to the nanoscale. Density functional theory (DFT) studies suggest that the unusual catalytic activity of these nanoparticles is associated with the presence of atoms with very low coordination number [17-18]. For example, Au nanoparticles having a size of 2-3 nm in diameter were well-known for their high catalytic activity for CO oxidation at or below ambient temperatures [19-20]. Nanosized gold particles in contact with support materials were found to exhibit high catalytic activity in number of reactions. Recently, it was further found that Au nanoparticles, as compared with Pt-group catalysts, are more selective towards various alcohols [21]. As in many other Au catalyzed reactions, smaller Au particles generally showed higher alcohol conversion due to their increased number of exposed Au atoms [22].

Gold is considered as a poor electrocatalyst particularly in acid medium. However, the electrocatalytic activity of gold in alkaline medium is quite high. Moreover, it was found that that the reaction intermediates such as CO do not poison gold surface [6]. It is known that the smooth gold surface shows poor electrocatalytic activity for alcohol oxidation reaction, while the activated rough surfaces show high electrocatalytic activity [23]. Different methods have been followed to produce rough gold surface onto substrates, which includes thermal treatment approach, underpotential deposition etc., [24-25].

Porous structures with large surface areas are technologically important as supports for catalysts, as membranes, in scaffolding applications, and as surface based sensors. In particular, noble metals with high surface areas are routinely used as catalysts, as substrates for surface-enhanced Raman spectroscopy etc., [26-39]. The most widely used technique for preparation of porous nanostructured metals is dealloying technique [40]. Very recently, there is a great deal of interest towards developing hydroxide ion conducting polymer membrane for DMFCs after the reported utilization of non-precious metals using such membranes in alkaline medium [41-43].

We have discussed in the previous chapter an *in situ* method of deposition of mesoporous gold on gold by novel electrochemical method without using templates. The deposited gold has been shown to possess very high surface area. In this chapter, we are extending our previous approach to deposit gold electrochemically on different substrates. We have deposited porous gold on platinum and graphite in addition to the gold on gold. The porous gold deposited surfaces were characterized by cyclic voltammetry, scanning electron microscopy, and surface XRD. The high surface area porous gold deposited on gold, platinum, and graphite surfaces were studied for electro-oxidation of alcohols in alkaline medium.

4.2 Experimental Section

4.2.1 Chemicals

All of the chemical reagents used in this study were analytical grade (AR) reagents. Sodium borohydride (Aldrich), KCl (Merck), 11-mercaptoundecanoic acid (Aldrich), ethanol (Merck) and methanol (Merck) were used as received. Millipore (Milli-Q) water having resistivity 18 MΩ cm was used to prepare all the solutions.

4.2.2 Surface Characterization

Scanning electron microscopy (SEM) characterization was carried out using a JEOL JSM- 840A model instrument with an energy dispersive X-ray (EDAX) attachment. Surface X-ray diffraction (XRD) measurements of surfaces coated with Au NPs were carried out using an Ultima X-ray diffractometer using Cu Kα radiation with a wavelength of 1.540 Å in grazing angle mode. The 2θ values were varied from 10 to 90°.

4.2.3 Electrochemical Instrumentation

The electrolysis was carried out using an EG&G potentiostat (model 263 A) interfaced to a computer through a GPIB card (National Instruments). This was used to control the current in a chronopotentiometry mode during the electrodeposition in a two electrode configuration. During CV and CA studies, the potentiostat was used in a normal three-electrode configuration with a platinum counter electrode, saturated calomel reference electrode and modified nanoparticles electrode as a working electrode.

4.2.4 Substrate Used for Deposition

We have used a 99.9% pure gold wire of 0.5 mm diameter and 5 mm exposed length as a sacrificial anode . The cathode is a gold disc of exposed area 0.002 cm^2 obtained by sealing a 0.5 mm diameter gold wire (Arora-Mathey) in soda lime glass, Pt wire of exposed area 0.125 cm^2 obtained by sealing in glass and graphite rod of exposed area 0.2 cm^2.

The electrodeposited samples were used for further electrochemical studies. We have also used the film coated on evaporated gold on glass (0.2 cm^2), Pt foil (0.2 cm^2), and graphite of 0.2 cm^2 for surface characterization studies such as SEM, EDAX, and XRD.

4.2.5 Electrode Pretreatment

The gold wire electrode was polished with emery papers of grade 800 and 1500, respectively, followed by polishing in aqueous slurries of progressively finer alumina of sizes ranging from 1.0 to 0.3 to 0.05 μm on a microcloth. After this, the electrode was ultrasonicated in Millipore Milli-Q water to remove alumina particles. Then, it was cleaned in a "piranha" solution, which is a mixture of 30% H_2O_2 and concentrated H_2SO_4 in 1:3 ratio. The polished gold wire electrode was thoroughly cleaned in distilled water followed by rinsing in Millipore Milli-Q water. This electrode is subjected to potential cycling between -0.5 and 1.4 V at a scan rate of 200 mV s^{-1} in 0.1M H_2SO_4 for about 20 cycles to effect electrochemical cleaning.

Before use, the Pt wire electrode was polished with emery papers of grade 800 and 1500, respectively, followed by polishing in aqueous slurries of progressively finer alumina of sizes ranging from 1.0 to 0.3 to 0.05 μm on a microcloth. After this, the electrode was ultrasonicated in Millipore Milli-Q water to remove alumina particles. Then, it was cleaned in conc. HNO_3. The polished Pt wire electrode was thoroughly cleaned in distilled water followed by rinsing in

Millipore Milli-Q water. This electrode is subjected to potential cycling between -0.5 and 1.4 V at a scan rate of 200 mV s^{-1} in 0.1 M H_2SO_4 for about 20 cycles to effect electrochemical cleaning.

Graphite rod with exposed surface area of 0.2 cm^2 was polished in 1000 emery sheet followed by polishing the graphite rod on smooth paper. The polished graphite rod was sonicated in Millipore Milli-Q water.

4.2.6 Electrodeposition of the Gold Nanoparticles Film on Gold, Platinum and Graphite Surface

An aqueous solution of 1M KCl in water, and 20 mM MUA in ethanol were mixed in equal proportion and stirred with a magnetic stirrer. The resulting clear solution was used as the electrolyte. The gold wire acts as an anode as well as the working electrode. The gold disc, Pt disc and graphite disc of geometric areas 0.002 cm^2, 0.125 cm^2, and 0.2 cm^2 respectively acts as cathode and the counter electrode in a two-electrode configuration. A distance of about 5 mm separates these two electrodes. The electrochemical dissolution of the gold wire and the simultaneous deposition of mesoporous gold on the cathode were carried out under constant current control in a chronopotentiometry mode at a room temperature of 25 °C. The electrolyte was stirred by means of a magnetic stirrer during the deposition. The experiments were conducted at constant anodic current densities of 0.5 Acm^{-2} for 30 min duration for deposition of Au on Au and Au on Pt, whereas 60 min duration was conducted to deposit Au on graphite. The dissolution of gold is accompanied by evolution of gases on both of the electrodes due to the electrolysis of water. Therefore, the electrochemical cell should have openings on the cell close to the electrodes to allow the gases to escape. Simultaneously, the gold wire starts to dissolve within a few minutes.

4.2.7 Cyclic Voltammetry Studies

Alcohol oxidation reactions were carried out using CV and CA. CVs were carried out at different concentrations from -600 mV to +600 mV vs SCE. CV results reported are either 2 cycles data or 200 cycles data. The experiments were carried out in order to understand the behavior of a fresh and clean electrode in the beginning of the scan, an information that could be obtained from the 2

cycle. The information on any possible adsorbed intermediates formed during the methanol oxidation contaminating the surface could be gathered from the 200th cycle CV.

4.2.8 Chronoamperometry Studies :

Prior Potential programme for the Chronoamperometry- Potential –current plots :

For the collection of current - potential data, the chronoamperometry measurements were carried out. In this procedure, a potential step is applied to the electrode surface and the steady state current after a duration of 20 seconds is collected. By varying the potential step, current values are measured at different potentials. This provides the necessary data for the construction of current – potential plot which is also called Tafel Plot.

However there is a problem associated with the potential-current measurements in alcohol oxidation studies due to the strong adsorption of the reaction intermediates during the application of potential step. If these adsorbed intermediates are not removed completely, the subsequent potential pulse will encounter a contaminated surface and the resulting current value will not reflect the reaction on a clean surface. Therefore a method has to be evolved to pre-clean the surface before the application of each potential step. The following method is followed to achieve this objective **[50-51].**

We have used a procedure of applying a prior potential program of a particular sequence just before the application of every potential step for CA studies. The advantage of prior potential programming is that it can be effectively used to remove the adsorbed intermediates which are formed during alcohol oxidation. This procedure results in a fresh surface for the chronoamperometry pulse to be applied for studying alcohol oxidation reaction and collecting the potential-current data for the Tafel plot studies. The fresh surface also makes available more adsorption sites for the reaction to take place.

Figure 1 shows the schematic of the potential programming used in CA studies. First, a positive potential of +0.9 V of 5 sec duration is applied. This positive potential desorbs and removes the adsorbed intermediates formed during the previous CA pulse. Though this will create a fresh surface free from intermediates, the surface oxides will be formed due to the applied positive potential. Therefore, the next step is the application of a negative potential of -0.6 V which will reduce the surface oxides that would have been formed during the positive potential pulse. This process finally will result in a pristine surface. Immediately, the desired CA

pulse of 20 sec duration is applied to collect the current- potential data. The whole sequence is repeated before the application of each CA pulse of increasing potential. The CA experiments carried out in this manner is denoted in this chapter as 'with prior potential programming'.

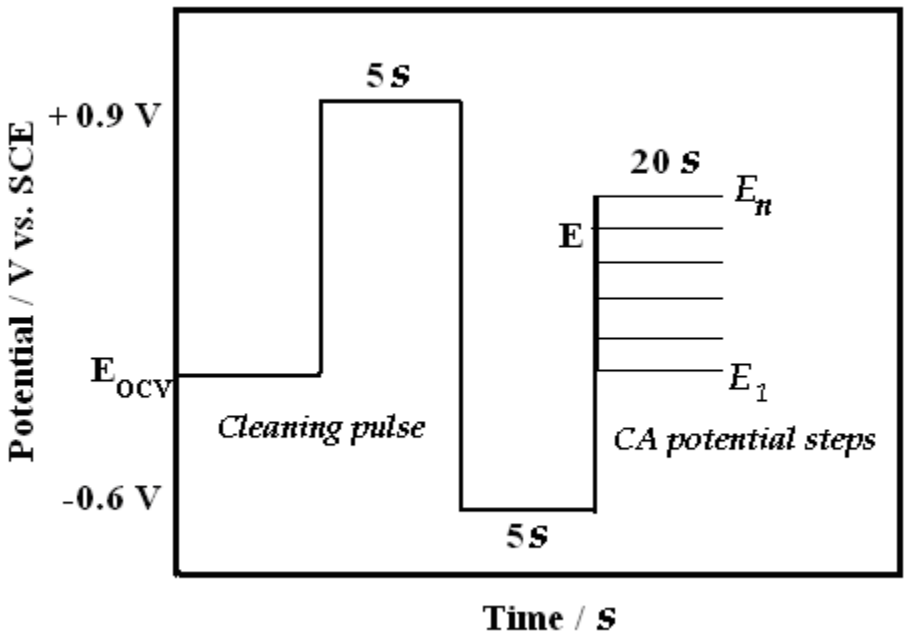

Figure 1. The schematic of the potential program used in chronoamperometry. E_{ocv} denotes the open circuit potential and E_1 …. E_n denote the CA potential steps . The value of E is incremented in steps of + 10 mV up to + 90 mV to collect the current - potential data.

Therefore, the CA studies on all the surfaces (Au/Au, Au/Pt, Au/C) are carried out in two different experimental conditions:

a) With prior potential programming: First applied the potential program (Figure 1) for the reasons explained above. This is followed by the application of a CA potential pulse of 20 sec duration from -0.6 V to the onset potential (zero overpotential) and then in steps of + 10 mV up to + 90 mV overpotential. The current values are collected at the end of 20 sec

b) Without potential programming: By the application of step pulse of 20 sec duration from the onset potential (zero overpotental) in steps of + 10 mV up to + 90 mV. The current values are collected at the end of 20 sec.

4.3 Results and Discussions

4.3.1 Methanol and Ethanol Electro-Oxidation Reaction on the Mesoporous Gold on Gold Surface

In order to demonstrate the electrocatalytic activity of the gold nanoparticle coating, we take alcohol electro-oxidation reactions on the mesoporous electrode (30 min deposition time) in an alkaline medium as model systems. The mesoporous electrode is known to be a more potent electrocatalyst than the bulk gold surface for the oxidation of alcohols in alkaline media, and several groups have studied this system, as it has the potential to be used in direct alkaline alcohol fuel cells and electrochemical sensors [43-47].

Assiongbon *et al.* proposed a general mechanism for the methanol oxidation reaction in alkaline medium is as follows [6].

Initially, chemisorption of OH^- on the gold surface takes place. This adsorbed OH^- plays a major role in the surface electrochemistry of Au in alkaline medium.

$$Au + OH^- \longrightarrow Au\text{-}OH^{(1-\lambda)-} + \lambda e^-$$

The intermediate steps for methanol oxidation is as follows

$$CH_3OH + Au\text{-}OH^{\delta-} \longrightarrow Au\text{-}OH^{\delta-}\text{-}CH_3OH \qquad \text{where, } \delta = (1-\lambda)$$

$$Au\text{-}OH^{\delta-}\text{-}CH_3OH \longrightarrow Au + H_2O + {}^{\cdot}CH_2OH + \delta e^-$$

$${}^{\cdot}CH_2OH + 4OH^{x-} \longrightarrow HCOO^- + 3H_2O + (4x)e^-$$

The net reaction for the methanol oxidation reaction is

$$CH_3OH + Au\text{-}OH^{\delta-} + 4OH^{x-} \longrightarrow Au + HCOO^- + 4\,H_2O + (\delta\text{-}1+4x)e^-$$

4.3.1.1 Cyclic Voltammetry (CV) Studies

Methanol Oxidation Reaction

Figure 2 shows the CVs for the methanol oxidation reaction on mesoporous gold in 0.5 M NaOH. The CV of mesoporous gold in the absence of methanol in 0.5 M NaOH is shown in Figure 2a, while Figure 2b corresponds to that of methanol electro-oxidation in the same medium

at a concentration of 2 M methanol. It is known that the methanol oxidation reaction involves the following primary step of generation of formate ions according to the reaction [43].

$$CH_3OH + 5OH^- \longrightarrow HCOO^- + 4H_2O + 4e^- \quad (1)$$

A small hump with a peak potential at -0.270 V verses SCE seen in Figure 2b corresponds to the above process. Similar behavior was observed in the case of methanol electro-oxidation on Pt modified nanostructured porous gold [42] and carbon supported and thermally activated Au-Pt nanoparticles immobilized on a glassy carbon electrode [44]. When the scanning is continued toward a more positive potential range, the cyclic voltammogram shows a high oxidation current around +0.175 V verses SCE which is attributed to the oxidation of the formate formed at -0.270 V verses SCE, as shown in (1) to carbonate as shown below [6].

$$HCOO^- + 3OH^- \longrightarrow CO_3^{2-} + 2H_2O + 2e^- \quad (2)$$

A strong OH^- ion adsorption at these potential ranges is connected with the higher electrocatalytic activity which has been shown to be sensitive to the shape and size of crystallites and the crystallographic orientation [6,43]. The electrocatalytic activity of gold decreases with prolonged potential cycling and remains constant after about 200 cycles, as shown in Figure 2c. This shows that, though the film is stable, there is a significant loss of electrocatalytic activity during potential cycling. This is indicative of trapping of some intermediates during the electro-oxidation within the pores.

Figure 2 (inset) shows the plot of the peak currents at different concentrations of methanol measured at the peak potential of +0.175 V verses SCE. Clearly, there are large number of active sites available for the methanol oxidation without surface saturation even at a relatively high concentration of 2 M methanol. The peak current due to methanol oxidation for 2 M methanol is measured to be about 0.22 mA. This is a very large current for such a small electrode with a geometric area of 0.002 cm^2 but can be readily understood if one realizes that the electroactive true surface area after deposition is 0.9 cm^2.

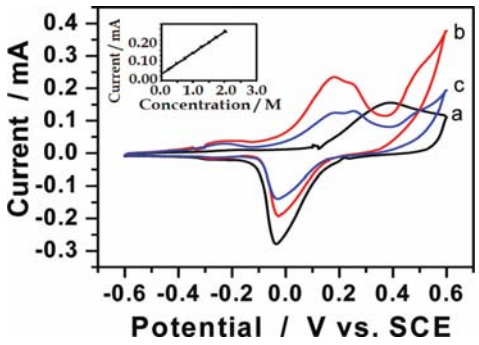

Figure 2. Cyclic voltammograms at a scan rate of 100 mV s^{-1} recorded for mesoporous Au NPs on Au in (a) 0.5 M NaOH, (b) 0.5 M NaOH + 2.0 M methanol, and (c) in 0.5 M NaOH + 2.0 M methanol after 200 cycles. Inset: Peak currents at +0.175 V verses SCE for a mesoporous coated gold electrode in 0.5 M NaOH with different concentrations of methanol. The current intercept in the absence of methanol corresponds to the gold surface oxidation current.

Ethanol Oxidation Reaction

There are a few reports of electro-oxidation studies of ethanol on gold in an alkaline medium compared to that of methanol [53-54]. de Lima and Varela have found by *in situ* FTIR spectroscopy that the acetate ion is the primary product of the ethanol oxidation reaction on gold in an alkaline medium, an observation in agreement with the earlier reports [53]. The reaction in the case of ethanol oxidation is

$$CH_3CH_2OH + 5OH^- \longrightarrow CH_3COO^- + 4H_2O + 4e^- \qquad (3)$$

The cyclic voltammogram of Figure 3 shows the ethanol oxidation process in 0.4 M ethanol in 0.5 M NaOH. The open circuit potential for ethanol oxidation is -468 mV verses SCE while the onset potential for ethanol oxidation is -300 mV which means that the over potential for ethanol oxidation is about 168 mV. It can be seen that the electro-oxidation starts at a potential of -300 mV verses SCE and the current attains the maximum value at a potential of +150 mV. The potential at which the ethanol oxidation peak occurs is somewhat more negative by 25 mV than that of methanol oxidation in 0.5 M NaOH. The inset shows the plot of the peak current verses ethanol concentration up to a concentration of 0.4 M, showing linear response. In Figure 3 curve a shows the cyclic voltammogram of the mesoporous gold surface, and curve b, the cyclic voltammogram after 200 cycles of scanning within the potential range. There is a decrease in the peak current after the potential cycling. Curve c shows that the performance of the electrode is partially regained immediately after cleaning and rinsing with Milli Q water. This shows that a simple rinsing process can easily renew the electrode surface without significant loss of activity.

Reaction Kinetics of Au NPs on Au Electrode for Methanol and Ethanol Oxidation Reaction

An Arrhenius plot displays the logarithm of current (log *i*) plotted against inverse temperature (1 / *T*). Arrhenius plots are often used to analyze the effect of temperature on the rates of chemical reactions. For a single rate-limited thermally activated process, an Arrhenius plot gives a straight line, from which the activation energy can be calculated using the slope = -*E*a/(2.3*R*) [48-49].

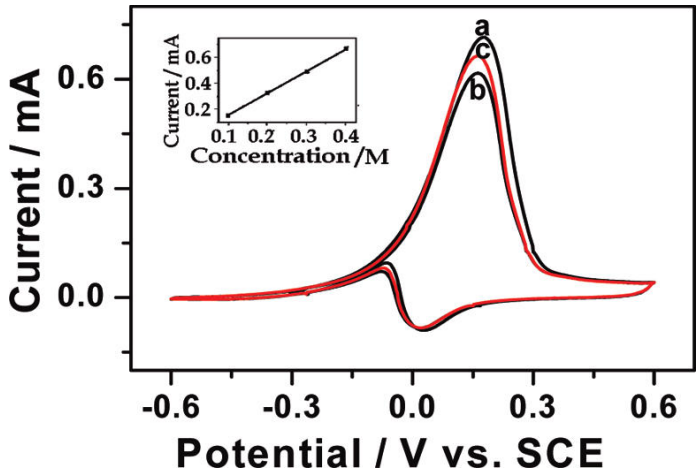

Figure 3. Cyclic voltammograms at a scan rate of 100 mV s^{-1} recorded for A/Au in (a) 0.5 M NaOH + 0.4 M ethanol and (b) 0.5 M NaOH + 0.4 M ethanol after 200 cycles. (c) The same electrode used in part b is taken out, washed, and reused in the same electrolyte. Inset: Plot of the peak currents measured at +0.150 V verses SCE for a mesoporous gold electrode in 0.5 M NaOH with different concentrations of ethanol.

The Arrhenius plots for methanol oxidation on Au/Au in 2.0 M CH_3OH + 0.5 M NaOH aqueous solution at different potentials are shown in Figure 4, where *i* is the current at a scan rate of 100 mV s^{-1}. The plots for ethanol oxidation reaction on Au/Au in 0.4 M CH_3CH_2OH + 0.5 M NaOH aqueous solution at different potentials are shown in Figure 5. It can be observed that these plots possess a very good linear relationship. The activation energy allows the reaction to proceed under milder conditions and thus is particularly beneficial in achieving the long-term stability of the catalysts. The activation energy decreases with increasing temperature, which is due to the increasing rate of the reaction with increasing temperature.

The E_a values for methanol and ethanol oxidation reactions are mentioned in the brackets of figure captions of Figure 4 and 5. As can be seen, the activation energies of ethanol oxidation reaction are less than the methanol oxidation reactions on Au/Au electrode. This shows that the ethanol oxidation reaction on Au/Au is thermodynamically more favored compared to the methanol oxidation reaction.

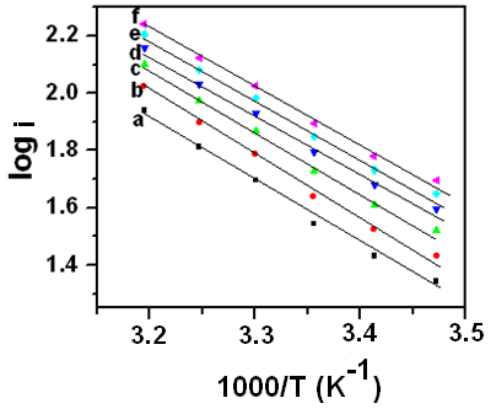

Figure 4. Arrhenius plots for 2M methanol oxidation reaction in 0.5 M NaOH on Au NPs on Au surface at different potentials (a) 40 (E_a = 42.2 kJ mol^{-1}), (b) 60 (E_a = 41.2 kJ mol^{-1}), (c) 80 (E_a = 40.7 kJ mol^{-1}), (d) 100 (E_a = 39.5 kJ mol^{-1}) (e) 120 (E_a = 39.2 kJ mol^{-1}), and (f) 140 (E_a = 38.3 kJ mol^{-1}) mV.

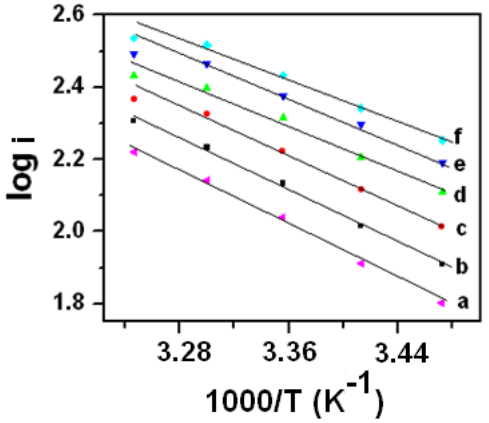

Figure 5. Arrhenius plots for 0.4 M ethanol oxidation on mesoporous Au NPs on Au at different potentials (a) 0 (E_a = 36.3 kJ mol^{-1}), (b) 20 (E_a = 34.4 kJ mol^{-1}), (c) 40 (E_a = 31.1 kJ mol^{-1}), (d) 60 (E_a = 28.5 kJ mol^{-1}) (e) 80 (E_a = 26.1 kJ mol^{-1}), and (f) 100 (E_a = 25.2 kJ mol^{-1}) mV

4.3.1.2 Chronoamperometric Studies

Methanol Oxidation Reaction

Chronoamperometry for the methanol oxidation reaction has been carried out with and without a prior application of potential programming. As explained in section 4.2.8, the CA with prior potential programming was carried out to effect the electrochemical cleaning.

The Tafel plots for the methanol and ethanol oxidation reactions without and with prior potential programming are shown in Figure 6 and Figure 7. It can be seen that for a given potential the current values are higher when a potential program is applied. This is because the application of prior potential program removes the surface contaminations and provides a clean surface for the application of CA pulse. This results in higher currents as seen in Figure 7.

Behavior of Tafel Slope Values as a Function of Temperature

Tafel slopes determined at different temperatures are shown in the Table 1 and Table 2. The Tafel slopes determined for oxidation of alcohols on metal surfaces have different connotation and do not have the same explanation as normally explained for simpler reactions on a clean electrode surface. This is because of the intense surface contaminations due to the formation of various intermediates which adsorb irreversibly on the metal surfaces during alcohol electro-oxidation [47].

It can be seen from the Table 1 and Table 2 the values of Tafel slopes are very large (> 200 mV/dec). Such large values of Tafel slopes are due to the surface contamination by the intermediates formed during the methanol oxidation reaction. This phenomenon can be explained as follows:

The Tafel slope is defined as ($d\eta/d\log i$) where η is the overpotential and i is the current density. This means that when a larger overpotential is applied for a given value of current to flow, the value of Tafel slope is also high. On a contaminated surface, the active surface sites are depleted. That means that significantly more overpotential has to be applied for a defined value of current to flow.

It can be seen from the Table 1 and Table 2 that the measured Tafel slopes for methanol and ethanol oxidation reactions increase with temperature. The reason for increase of Tafel slopes with temperature is as follows :

As the temperature increases the rate of the reaction proportionately increases following Arrhenius equation. This results in more reaction products being formed. This also means that

the concentration of reaction intermediates is more at higher temperatures. These reaction intermediates irreversibly adsorb and block the reaction sites. In other words more overpotential has to be applied at higher temperatures for a defined current to flow. This phenomenon increases the Tafel slopes at higher temperatures as observed in Table 1 and Table 2.

Variation in Tafel Slopes With and Without Prior Potential Programming

Table 1 and 2 also presents the Tafel slopes with and without potential programming for methanol and ethanol oxidation reactions respectively. It can be seen that the Tafel slopes for both methanol and ethanol oxidation reactions are higher when a prior potential program is applied. This is due to the prior cleaning of the electrode surface by potential program before the application of CA pulse. As explained earlier this results in higher oxidation currents. This means more reaction products are formed and more reaction intermediates which adsorb irreversibly on the surface. This again results in increased Tafel slopes as observed in the Table 1 and Table 2. It may be also noted that the Tafel slopes are very much higher for ethanol oxidation (Table 2) compared to the values for methanol especially at higher temperatures. This phenomenon can be explained as due to the formation of higher amount of carbonaceous intermediate species in the case of ethanol as it has an extra methylene ($–CH_2$) group.

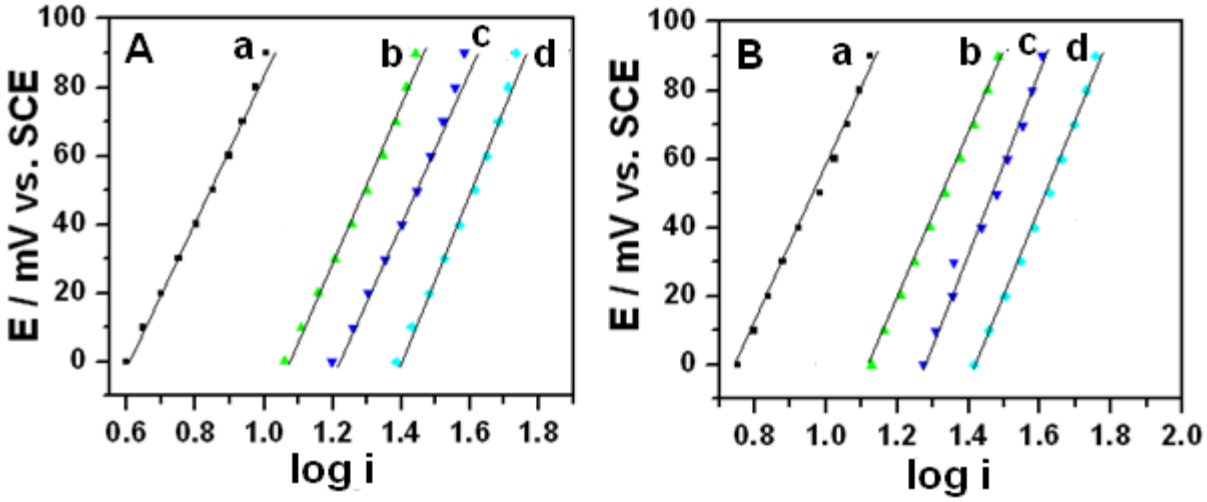

Figure 6. Tafel plots for Au/Au in 2 M methanol oxidation reaction and 0.5 M NaOH, (A) without and (B) with potential programming at (a) 15 ^{0}C, (b) 25 ^{0}C, (c) 30 ^{0}C, and (d) 35 ^{0}C.

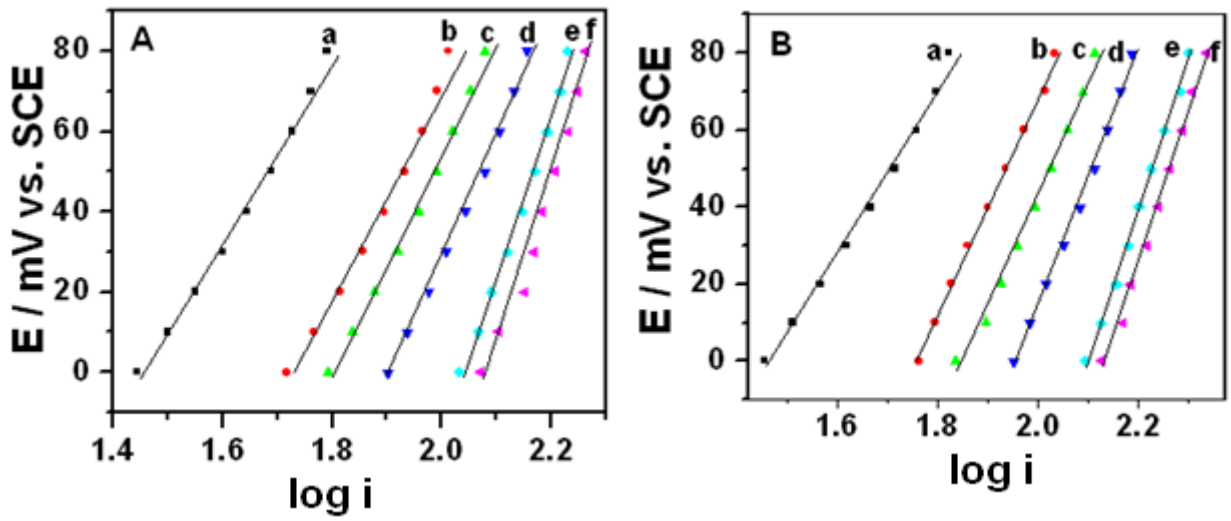

Figure 7. Tafel plots for Au/Au in 0.4 M ethanol oxidation reaction and 0.5 M NaOH (A) without and (B) with potential programming at (a) 15 ^{0}C, (b) 20 ^{0}C, (c) 25 ^{0}C, (d) 30 ^{0}C, (e) 35 ^{0}C, and (f) 40 ^{0}C.

Temperature (^{0}C)	Tafel slope (mV/dec)	Tafel slope (mV/dec) (with potential programming)
15	215	234
25	228	247
30	231	256
35	249	260

Table 1. Tafel slopes determined from chronoamperometry on Au/Au for 2 M methanol oxidation reaction in 0.5 M NaOH without and with potential programming.

Temperature (^{0}C)	Tafel slope (mV/dec)	Tafel slope (mV/dec) (with potential programming)
15	227	212
20	264	285
25	277	294
30	309	332
35	396	391

Table 2. Tafel slopes for 0.4 M ethanol oxidation reaction determined from chronoamperometry on Au/Au without and with potential programming.

4.3.2 Alcohol Oxidation Studies of Porous Gold Deposited on Pt and Graphite Surfaces

Pt is a good catalyst for methanol oxidation reaction in acid medium. Because of the adsorption of reaction intermediates onto the Pt surface, methanol oxidation reaction is limited on the Pt metal. It is worth discussing here the mechanism of methanol oxidation on Pt surface in acid medium. There are two types of possible mechanisms for methanol oxidation reaction on Pt. One is direct and another is indirect mechanism as proposed by Ferrin *et al.* [55].

The first step in the reaction mechanism is the activation of methanol molecule via hydrogen abstraction from either the carbon or the oxygen atoms. Further hydrogen abstraction steps can create formaldehyde or hydroxymethylene (CHOH), followed by formyl or COH. In the direct mechanism, rather than stripping off the final hydrogen from COH or CHO to form CO, a proton/electron pair will be stripped off of a water molecule, and the resulting OH group binds with the carbonaceous species to form di-oxygenated species (dihydroxycarbene ($C(OH)_2$) or formic acid (HCOOH). This hydroxyl addition is followed by dehydrogenation to either formate (HCOO) or carboxyl (COOH), with subsequent dehydrogenation to the final product. An alternative direct pathway involves the stripping of a proton/electron pair from water and addition of the resulting hydroxyl to formaldehyde, to form H_2COOH, which can then be dehydrogenated to formic acid or dioxymethylene (H_2COO). Dioxymethylene can then be dehydrogenated to formate and ultimately to CO_2.

In the indirect mechanism, the CHO or COH are directly dehydrogenated to CO. Water is dissociated separately on the surface to form OH, and the two surface species react together to form CO_2(g) in a manner analogous to the water-gas-shift reaction. The intermediates CH_2OH* binds to the Pt via carbon whereas, CH_3O* binds via oxygen. CH_2OH* is more stable than CH_3O*, this is because Pt binds carbon more strongly than oxygen. The affinity of Pt for carbon also explains the stability of CHOH* and COH* (both of which bind through carbon), the next intermediates in the most stable reaction pathway. The CO* is the most stable intermediate on the Pt which results in the poisoning of Pt surface. As the potential is high enough to overcome the thermodynamic barrier to activate methanol, all subsequent steps leading to CO* are lower in free energy. The steps following CO*, however, has a very large thermodynamic barrier.

Several attempts were made to overcome the adsorption of intermediates especially CO, for example by the use of Pt based alloys [56], Ru-decorated Pt [57], non-Pt catalyst [58], and

thin films of Pt [56-60]. Depending on the chemical and physical properties of the substrate, the catalytic activity of the thin film deposited on the surface changes.

Gold has attracted an enormous interest recently due to possibility of using alternative to platinum. Gold has a filled d-orbital and a relatively low (energetically) d-band center as compared to the other transition metals, which provides gold with stability. Recently, Zhang *et al.* have reported the stabilization effect on the activity of Pt by Au clusters deposited on the surface [61]. Here, the Au clusters were deposited on a Pt catalyst (carbon-supported Pt nanoparticles) through galvanic displacement by Au of a Cu monolayer on Pt. This has been postulated as the change of surface Pt d-bands after gold clusters deposition [61, 62-64].

It is interesting to study the Pt coated gold for methanol oxidation reactions. It is also important to study the deposition of gold on graphite surface, as graphite surface is very cheap and hence finds application in low cost commercial devices. We have deposited Au on Pt and graphite surface electrochemically. The deposited gold is porous in nature and shows high surface area. Au deposited on Pt has been characterized using SEM, XRD, and CV. We have examined the high surface area of Au on Pt for alcohol oxidation reaction using CV and chronoamperometry.

4.3.2.1 Surface Characterization Using SEM

The electrochemically coated Au on Pt and graphite surfaces were characterized using SEM. Figure 8 shows the SEM images of Au on Pt for different deposition times. The SEM images show clusters of gold which are deposited on the surface. With increasing deposition time, density of deposited gold clusters increases. Fractal type growth of gold has been observed for 60 minutes deposition time. With further increasing time of deposition (90 minutes of deposition time), the gold grows like a mesh type structure. The high resolution image of the mesh shaped gold structure consists of nanometer sized particles. This kind of small size gold particle deposition is almost similar to the gold deposition on gold. This shows that sufficient thickness of gold has been formed to completely cover the Pt surface. The completely covered gold on platinum surface provides lesser nucleation sites for the further deposition of Au. This indicates that the lattice constants of the substrate play an important role in depositing the nano sized particles.

Figure 9 shows the energy dispersive X-ray (EDAX) of the Au deposited on Pt for 30 minutes duration. EDAX shows that the 84.5 and 12.1 weight percentages of Au and Pt are present in the clusters respectively. In addition to the gold there are some electrolytes residues which have been formed in the Au NPs film which are 2 and 2.4 weight percentages of oxygen and chlorine respectively.

Figure 10(I) is the SEM image of the bare graphite surface. Figure 10(II) is the SEM image of the Au deposited on graphite for 60 minutes electrochemically. The image shows granular clusters of Au particles on graphite surface. Figure 11 shows the EDAX of the Au NPs deposited on graphite from which 59.7 % C (by weight) and 35 % Au (by weight) has been obtained. The large amount of carbon atoms arise from the underlay carbon substrate can also be seen. This large amount of carbon from the substrate is due to the highly porous nature of the film. The impurities in the Au film were Cl and O which are about 2 and 2.9 % (by weight) respectively.

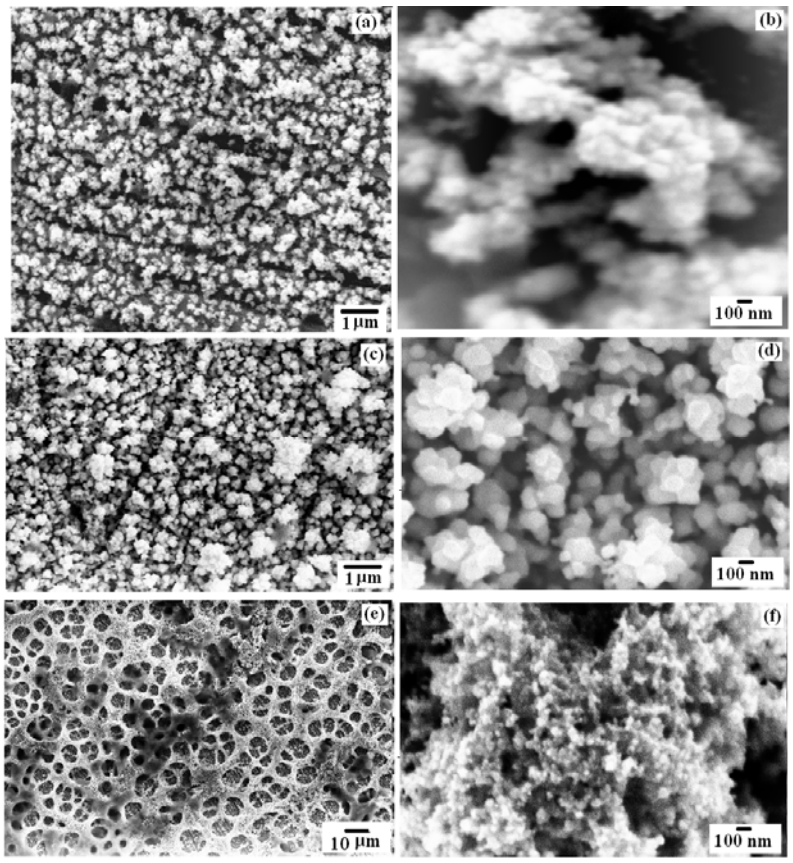

Figure 8. SEM images of Au/Pt surface using MUA and KCl at (a) 30, (c) 60 and (e) 90 minutes of deposition time and corresponding higher magnification images are (b), (d) and (f) respectively.

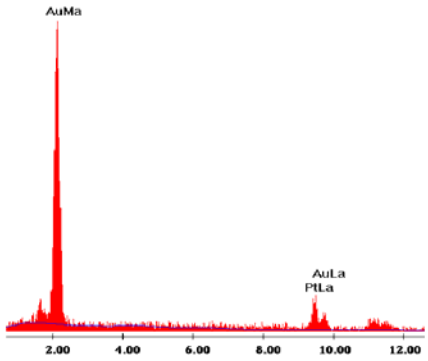

Figure 9. EDAX of Au/Pt for 30 minutes of deposition using MUA and KCl.

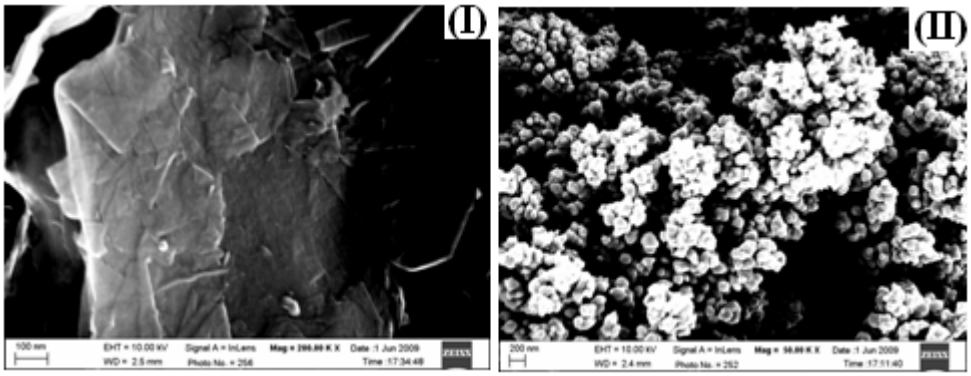

Figure 10. SEM images (I) bare graphite substrate (II) Au on graphite deposited electrochemically using KCl and MUA.

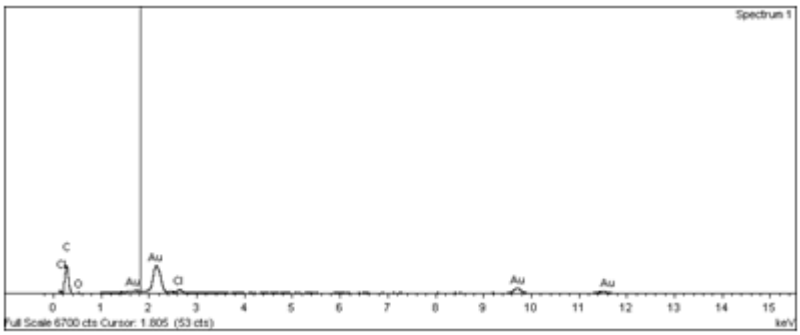

Figure 11. EDAX of the Au deposited on graphite.

4.3.2.2 Surface X-ray Diffraction (XRD) Studies

Surface X-ray diffraction measurements of Au deposited on Pt and graphite surfaces were carried out using Cu Kα radiation with a wavelength of 1.540 Å. The 2θ values were varied from 10^o to 90^o.

The XRD of the Pt substrate is shown in the Figure 12a. The Pt substrate showed clear reflections at angles (2θ) of 39.8, 46.3, 67.5 and 81.3 that are associated with the [111], [200], [220] and [311] facets of Pt crystallites, respectively [65-66].

Figure 12b shows the surface XRD of Au on Pt. The Au on Pt shows the reflections at angles (2θ) of 38.2, 44.3, 64.7, and 77.5 that are associated with the [111], [200], [220] and [311] facets of Au crystallites, respectively. It can also be seen that the reflections from the Au are same as that of bulk gold which are indexed to the face centered cubic (fcc) structure of Au. The broadened XRD peaks for the Au on Pt surface compared to the sharper bulk gold XRD [67], indicates the presence of nanometer sized clusters on the Pt surface.

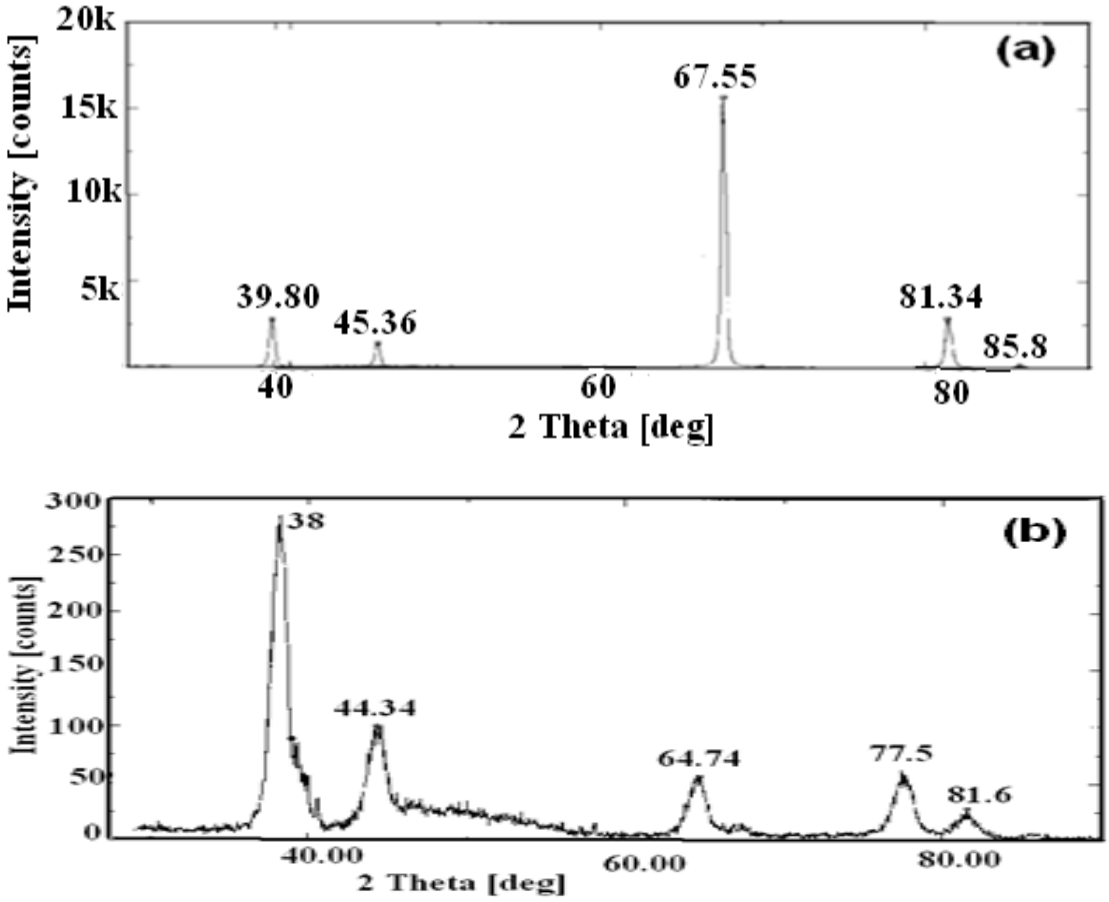

Figure 12. XRD of (a) polycrystalline Pt substrate and (b) Au on Pt grown electrochemically in presence of MUA and KCl.

The XRD of the graphite substrate is shown in Figure 13a. The graphite substrate showed clear reflections at angles (2θ) of 26.55, 42.62, 44.58, 77.62, and 83.69. Figure 13b shows the surface XRD of Au on graphite. The Au on graphite shows the reflections at angles (2θ) of 21.21, 23.58, 38.21, and 64.46 in addition to the reflections from graphite substrate at 26.33, 42.33, 44.46, 77.46, and 83.71.

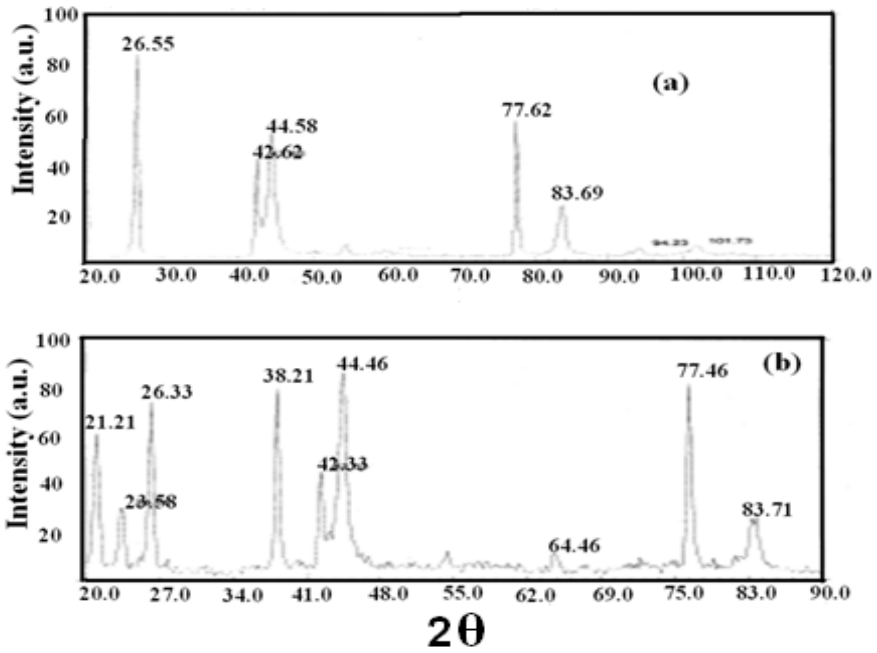

Figure 13. XRD of (a) graphite substrate and (b) Au on graphite grown electrochemically.

4.3.2.3 Electrochemically Determined Active Surface Area

We have determined the true surface area by cyclic voltammetry in 0.1 M $HClO_4$ by measuring the charge associated with the cathodic Au oxide stripping peak. Figure 14(I) shows the cyclic voltammograms in 0.1 M $HClO_4$ for Au deposited on Pt surface for 30 minutes of time. The voltammograms exhibit the typical behavior of polycrystalline Au in acid electrolyte with a clear Au oxide-stripping peak during the cathodic cycle. The real surface area of gold nanoparticles coated surface can be estimated from the amount of charge consumed during the reduction of Au surface oxide monolayer and the reported value is 390 μC cm^{-2} [68]. The electroactive surface area for the Au is thereby measured to be 0.34 cm^2 for 30 minutes deposition time for electrode of geometric area 0.125 cm^2. Table 3 summarizes the true surface area results for Au on Pt surface at different deposition time. The surface area increases with increasing deposition time, indicating the growth of the gold film.

Figure 14(II) shows the cyclic voltammograms in 0.1 M $HClO_4$ of Au on graphite for 60 minutes of deposition. The voltammograms exhibit the typical behavior of polycrystalline Au in acid electrolyte with a clear Au oxide-stripping peak during the cathodic cycle. The charge under reduction peak is 2.628 mC. The electroactive true surface area for the Au are thereby measured to be 6.7 cm^2 for 60 minutes deposition time.

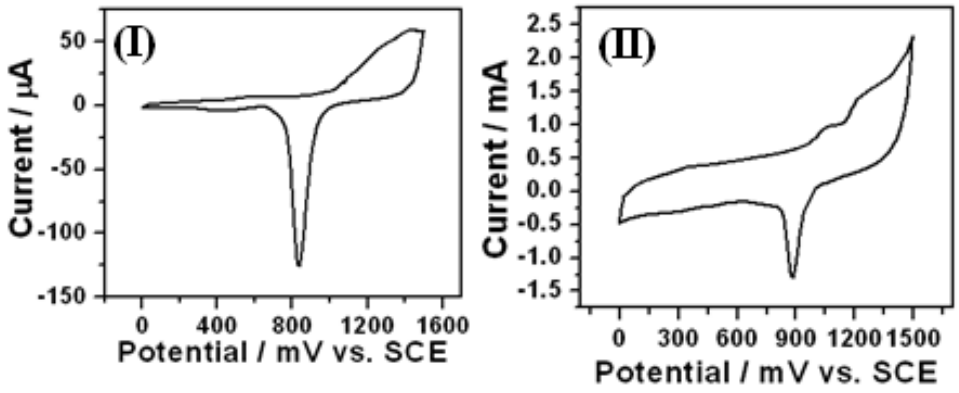

Figure 14. Cyclic voltammograms at a scan rate of 100 mV s^{-1} recorded in 0.1 M $HClO_4$ (I) Au on Pt and (II) Au on Graphite.

Deposition time (minutes)	Q (μC)	True surface area (cm^2)
30	134	0.34
60	430	1.10
90	600	1.56

Table 3. The true surface area of Au on Pt surface deposited for different deposition time.

4.3.3 Methanol and Ethanol Electro-Oxidation Reaction of Porous Au on Pt and Graphite Surface

Cyclic Voltammetry Studies

Figure 15 shows the CV of electro-oxidation of 2 M methanol in 0.5 M NaOH on bare Pt surface of geometric area 0.125 cm^2. The oxidation current continuously decreases with cycle number. Curve a is the CV of first cycle and curve b 200^{th} cycle. It shows that the methanol oxidation current decreases from 62 μA to 18 μA after 200 cycles. The decrease in oxidation current is due to the carbonaceous intermediates adsorbing onto the Pt surface during methanol oxidation reaction. As seen from curve c, methanol oxidation current does not increase even after washing the cycled Pt surface in 2 M methanol with a jet of water. This shows that adsorption of intermediates is very strong on Pt surface, which further hinder the oxidation of methanol.

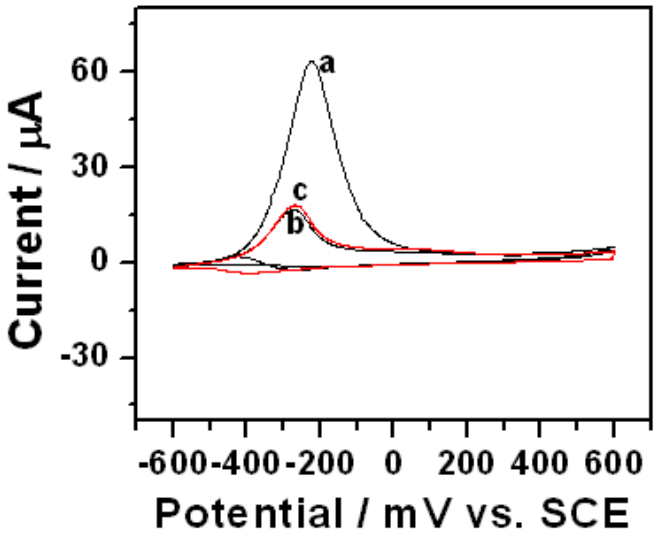

Figure 15. Cyclic voltammograms of bare platinum in 0.5 M NaOH with 2 M methanol at a scan rate of 100 mV s^{-1} a) 1st cycle, b) after 200 cycles, and c) after 200 cycles in methanol, electrode was washed with water and taken the CV in 2 M methanol and 0.5 M NaOH (geometric area of the electrode 0.125 cm^2).

Figure 16(I) shows the typical CVs of Au/Pt electrode in 0.5 M NaOH solution containing different concentration of methanol at a scan rate of 100 mV s^{-1}. In methanol free solution CV shows an oxidation wave at 250 mV, attributed to the formation of surface gold oxides. With increasing concentration of the methanol, oxidation peak current increases. It is clear from CV that methanol oxidation takes place at two different potentials. The first region is from -500 to +150 mV verses SCE which is corresponding to the oxidation of methanol into formate ion. The second region is at +170 to +300 mV verses SCE which corresponds to the conversion of formate into carbonate ion. The onset potential for methanol oxidation occurs at -500 mV verses SCE. A large anodic peak current was observed at -130 mV, representing the highest rate of catalytic oxidation of methanol. The peak current density for the 2 M methanol oxidation is 0.61 mA cm^{-2}. This current density is higher than the polycrystalline gold electrode and in the range reported for porous gold electrode [19,37]. The open circuit potential for methanol oxidation is -605 mV verses SCE which means that the overpotential for methanol oxidation is about 105 mV. In comparison to the Au on Au, the onset potential of Au on Pt for methanol oxidation reaction occurs at more negative potential. The current due to first peak is smaller than the second peak in case of Au on Au. Whereas, the current due to first peak for Au

on Pt which is around -130 mV is higher than the second peak which occurs around +250 mV. This shows that the dominating reaction in the case of methanol oxidation on Au/Pt is the conversion of methanol to formate ion. The smaller peak at + 250 mV corresponds to conversion of formate to carbonate. This is one of the important results of this study.

Curve a in Figure 16(II) shows the first cycle CV of 2 M methanol oxidation and curve b shows after 200 cycles. The methanol oxidation current decreases from 225 µA to 50 µA after 200 cycles. However, the current regains to the almost to the value of first cycle, once the electrode was washed with water (curve c). Unlike on bare Pt surface where, the adsorbed intermediates could not be removed by washing with water. Figure 16(III) shows the plot of peak currents verses the concentration of methanol derived from the Figure 16(I).

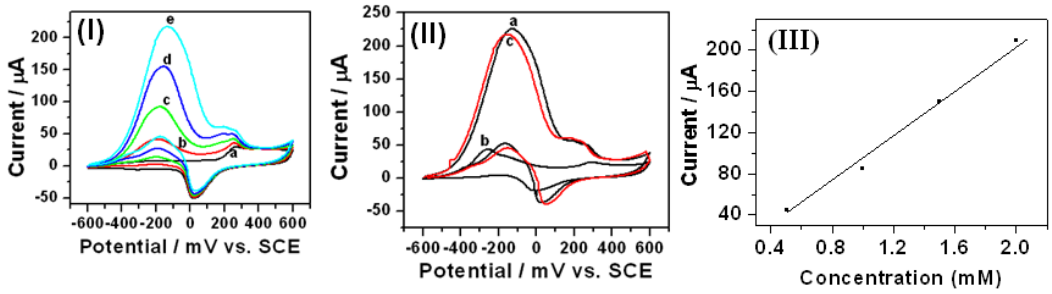

Figure 16. Cyclic voltammograms of Au/Pt in 0.5 M NaOH in methanol at a scan rate of 100 mV s^{-1} (I) a) 0 M, b) 0.5 M, c) 1 M, d) 1.5 M, and e) 2 M and (II) a) 1st cycle, b) after 200 cycles, and c) after 200 cycles in methanol, electrode was washed with water and taken the CV in 2 M methanol.

Figure 17(I) shows the cyclic voltammograms for the Au/C in 0.5 M NaOH. Concentration of methanol is increased in steps of 0.5 M. With increasing concentration of methanol, the oxidation current also increases. The current density for the methanol oxidation is 0.22 mA cm^{-2} for 2 M methanol. The OCP for the methanol oxidation is -222 mV verses SCE, while onset potential for the methanol oxidation is -100 mV verses SCE. Therefore, the overpotential is about 122 mV. The peak potential for methanol oxidation occurs at + 280 mV verses SCE which is highly positive compared to that of Au/Au (+175 mV) and Au/Pt (-130 mV). Figure 17(II) shows the CVs for the 2 M methanol oxidation for the first and 200th cycle. Upon cycling, about 25 % of the current decreases. This shows that the trapping of intermediates inside the porous structure of deposited Au. The decreased current does not regain even after

washing the electrode with water. This shows the adsorbed intermediates are strongly bound on the carbon support partially by chemisorption and could not be removed by simple washing. Figure 17(III) shows the plot of peak currents verses the concentration of methanol derived from the Figure 17(I).

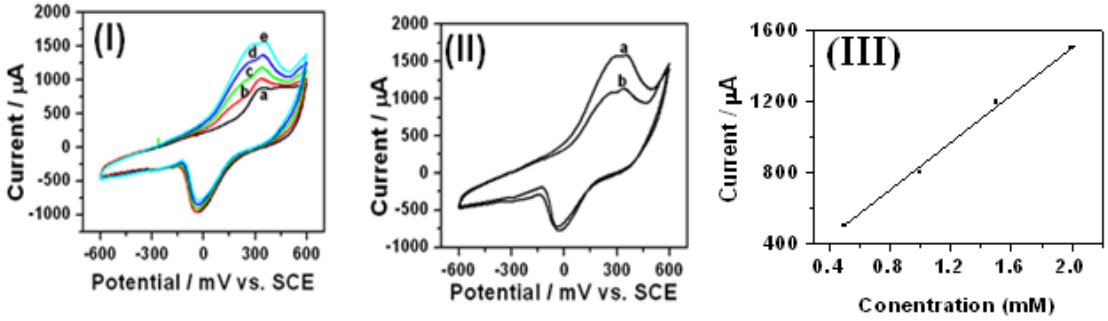

Figure 17. Cyclic voltammograms of Au/C in 0.5 M NaOH and methanol at a scan rate of 100 mV s^{-1} (I) a) 0 M, b) 0.5 M, c) 1 M, d) 1.5 M, e) 2 M (I), and (II) a) 1st cycle b) after 200 cycles.

Figure 18 shows the CVs of the bare Pt surface in 0.4 M ethanol and 0.5 M NaOH. It can be seen that the electro-oxidation starts at a potential of -0.6 V verses SCE and the current attains the maximum value at a potential of -0.3 V. The current due to ethanol oxidation decreases by about 6% upon cycling in 2 M ethanol for about 200 cycles. However, the 50% of the decreased current can be regained by washing the electrode with water and recycling in 0.4 M ethanol and 0.5 M NaOH.

Figure 19 shows the CVs of Au/Pt for ethanol oxidation reaction. The current due to ethanol oxidation increases with increasing concentration. The open circuit potential for ethanol oxidation is -702 mV and the onset potential for ethanol oxidation is -600 mV. The over potential for ethanol oxidation is about 102 mV, which is about 60 mV less compare to the ethanol oxidation on Au on Au. Curve a of Figure 19(II) shows the cyclic voltammogram of the porous gold on Pt in 0.4 M ethanol, and curve b is the cyclic voltammogram after 200 cycles of scanning within the potential range. There is a decrease in the peak current after the potential cycling. Curve c shows that more than 70 % of decreased current regained immediately after cleaning and rinsing the electrode with Milli Q water. This shows that a simple rinsing process can easily renew the electrode surface without significant loss of activity. Figure 19(III) shows the plot of peak currents verses the concentration of methanol derived from the Figure 19(I).

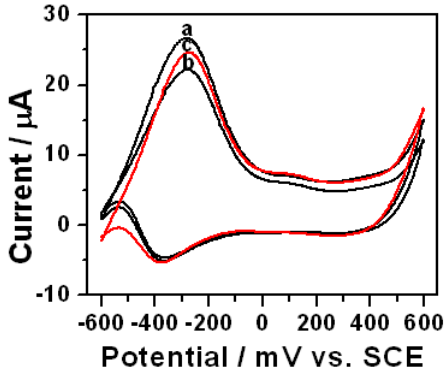

Figure 18. Cyclic voltammograms of bare platinum in 0.5 M NaOH with 0.4 M ethanol at a scan rate of 100 mV s^{-1} a) 1st cycle, b) after 200 cycles, and c) after 200 cycles in ethanol, electrode was washed with water and taken the CV in 0.4 M ethanol. (geometric area 0.125 cm^2)

Figure 20(I) shows the CVs of the Au/C for ethanol oxidation process with different concentrations in 0.5 M NaOH. The current increases with increase in concentration of ethanol. It can be seen that the electro-oxidation starts at a potential of -0.150 V verses SCE and the current attains the maximum value at a potential of +0.150 V verses SCE. The current density for ethanol oxidation is 16 mA cm^{-2}. The open circuit potential for ethanol oxidation is -353 mV verses SCE and the onset potential for ethanol oxidation is -150 mV verses SCE. The peak potential for ethanol oxidation is around 203 mV, which is more, compared to the ethanol oxidation on Au/Au or Au/Pt. Higher overpotential shows that ethanol oxidation of Au/C surface is less favored compared to the Au/Au or Au/Pt.

Curve a in Figure 20(II) shows the cyclic voltammogram of the Au/C in 0.4 M ethanol. There is a significant decrease in the peak current after the potential cycling (curve b). The 25 % of decreased current (Curve c) does not regain after cleaning and rinsing with Milli Q water. This shows that a simple rinsing process cannot easily renew the electrode surface. This is due to strong chemisorption of the reaction intermediates on the graphite substrate. Figure 20(III) shows the plot of peak currents verses the concentration of methanol derived from the Figure 20(I).

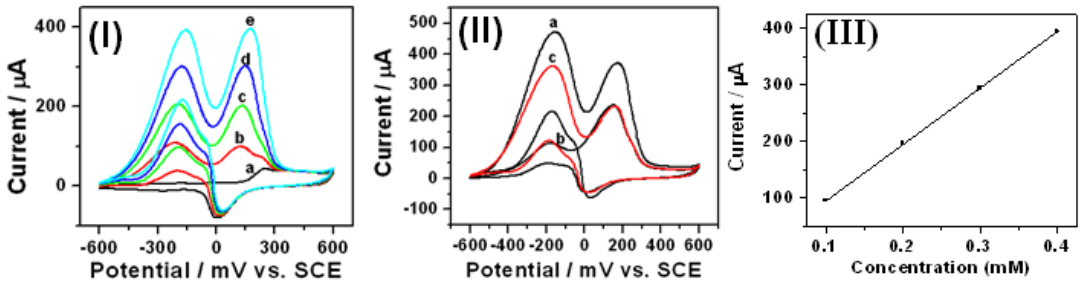

Figure 19. Cyclic voltammograms of Au/Pt in 0.5 M NaOH and ethanol at a scan rate of 100 mV s^{-1} (I) a) 0 M, b) 0.1 M, c) 0.2 M, d) 0.3 M, and e) 0.4 M of ethanol (II) a) 1st cycle, b) after 200 cycles, and c) after 200 cycles in ethanol, electrode was washed with water and taken the CV in 0.4 M ethanol.

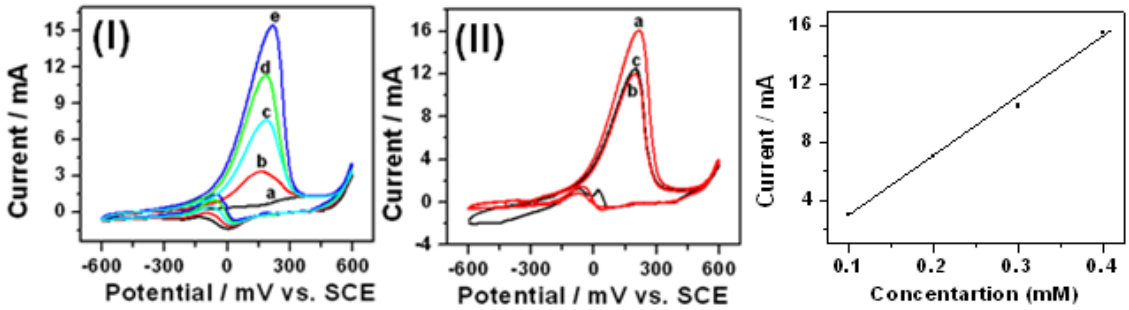

Figure 20. Cyclic voltammograms of Au/C in 0.5 M NaOH and ethanol at a scan rate of 100 mV s^{-1} (I) a) 0 M, b) 0.1 M, c) 0.2 M, d) 0.3 M, and e) 0.4 M (II) a) 1st cycle, b) after 200 cycles, and c) after 200 cycles in ethanol, electrode was washed with water and taken the CV in 0.4 M ethanol.

4.3.3.1 Reaction Kinetics of porous Au on Pt and graphite Electrode for Methanol and Ethanol Oxidation Reaction

Methanol Oxidation

The plots of log *i* versus 1/*T* for methanol oxidation on Au/Pt electrodes in 2.0 M CH_3OH and 0.5 M NaOH aqueous solution at different potentials are shown in Figure 18. The activation energies are in the range of 50-26 kJ mol^{-1}. The activation energy also decreases with increasing potential as seen in the Figure 21 which is to be expected as the rate of the reaction and therefore the current increases.

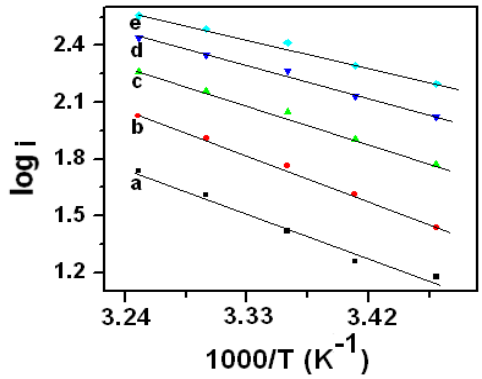

Figure 21. Arrhenius plots for 2 M methanol oxidation reactions of Au/Pt in 0.5 M NaOH at (a) -450 (E_a = 50.83 kJ mol^{-1}) mV, (b) -400 (E_a = 51.23 kJ mol^{-1}) mV, (c) -350 (E_a = 42.94 kJ mol^{-1}) mV, (d) -300 (E_a = 30.4 kJ mol^{-1}) mV, and (e) -250 (E_a = 26.5 kJ mol^{-1}) mV.

The Arrhenius plots for ethanol oxidation reaction of Au on graphite electrodes in 0.5 M NaOH aqueous solution at different potentials are shown in Figure 22. The activation energies are also shown in the brackets in the figure caption. The change in activation energy with increasing temperature is very much less compared to the change observed for methanol oxidation on Au on Au and Au on Pt surfaces. This shows the reaction rate is not significantly affected by increasing overpotential in the case Au on graphite substrate. This is also reflected in the larger overpotential needed to attain current maximum in the case of methanol oxidation on Au/C (Figure 17(I))

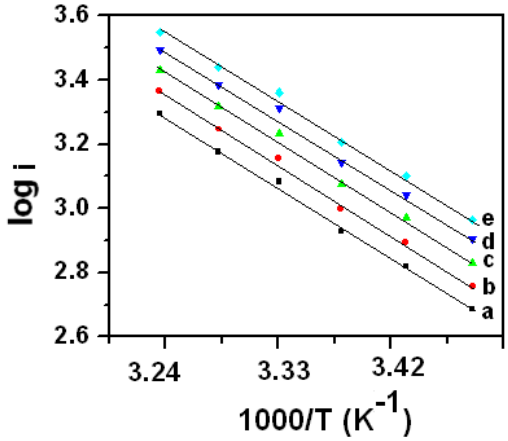

Figure 22. Arrhenius plots for 2 M methanol oxidation reactions of Au/C in 0.5 M NaOH (a) 40 (E_a = 42.27 kJ mol^{-1}), (b) 60 (E_a = 42.12 kJ mol^{-1}), (c) 80 (E_a = 41.39 kJ mol^{-1}), (d) 100 (E_a = 40.72 kJ mol^{-1}), (e) 120 (E_a = 40.47 kJ mol^{-1}) mV.

Ethanol Oxidation

The plots of log *i* versus 1/*T* for ethanol oxidation reaction of Au/Pt electrodes in 0.5 M NaOH aqueous solution at different potentials are shown in Figure 23. The activation energy decreases with increasing temperature, which is due to the increasing rate of the reaction with increasing temperature. The activation energies of ethanol oxidation reaction are in the range of 46-31 kJ mol^{-1}. The Arrhenius plots for ethanol oxidation reaction of Au/C electrodes in 0.5 M NaOH aqueous solution at different potentials are shown in Figure 24. The activation energies of ethanol oxidation reaction are in the range of 47-34 kJ mol^{-1} and it decreases with increasing temperature, as observed for other electrode systems.

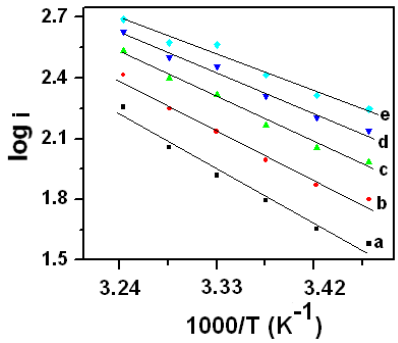

Figure 23. Arrhenius plots for 0.4 M ethanol oxidation reaction of Au on Pt in 0.5 M NaOH at (a) -450 (E_a = 46.29 kJ mol^{-1}) mV, (b) -400 (E_a = 42.79 kJ mol^{-1}) mV, (c) -350 (E_a = 38.71 kJ mol^{-1}) mV, (d) -300 (E_a = 34.57 kJ mol^{-1}) mV, and (e) -250 (E_a = 31.03 kJ mol^{-1}) mV.

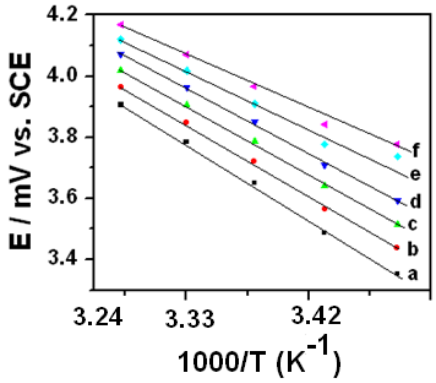

Figure 24. Arrhenius plots for 0.4 M ethanol oxidation reactions of Au on graphite in 0.5 M NaOH at (a) 100 (E_a = 47.8 kJ mol^{-1}) mV, (b) -80 (E_a = 45.34 kJ mol^{-1}) mV, (c) -60 (E_a = 43.27 kJ mol^{-1}) mV, (d) -40 (E_a = 41.18 kJ mol^{-1}) mV, (e) -20 (E_a = 34.21 kJ mol^{-1})mV, and (f) 0 (E_a = 34.2 kJ mol^{-1}) mV.

Chronoamperometric Studies

Methanol Oxidation

Chronoamperometry for the methanol oxidation reaction has been carried out with and without prior potential programming. Figure 25 shows the Tafel plots for the methanol oxidation reaction on Au/Pt and the results are presented in Table 4. The Tafel slope increases with increase in temperature. This aspect was discussed in the earlier section **[.....]**

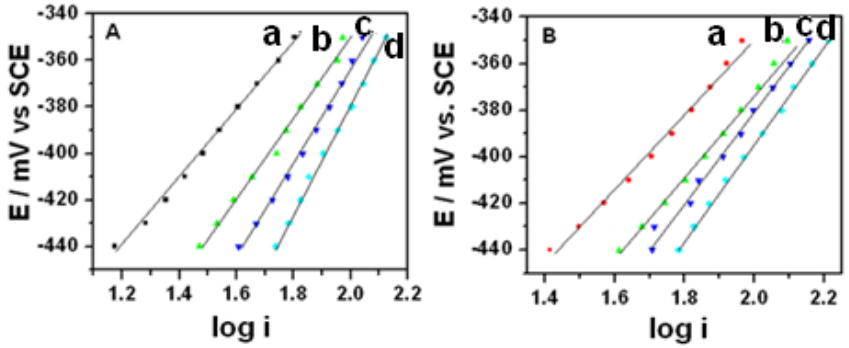

Figure 25. Tafel plots for 2 M methanol oxidation reactions in 0.5 M NaOH of Au/Pt (A) without and (B) with potential programming at (a) 15 ^{0}C, (b) 25 ^{0}C, (c) 30 ^{0}C, and (d) 35 ^{0}C.

Temperature (^{0}C)	Tafel slope (mV/dec)	Tafel slope (mV/dec) (with potential programming)
15	161	167
25	172	185
30	204	185
35	229	206

Table 4. Tafel slopes determined from chronoamperometry of Au/Pt for 2 M methanol oxidation reaction in 0.5 M NaOH without and with potential programming.

Figure 26 shows the Tafel plots for the methanol oxidation reaction of Au/C and the results are presented in Table 5. In this case the increase in Tafel slope with temperature is much more than for methanol oxidation reaction on Au/Au and Au/Pt. This is because on Au/C the adsorbed intermediates are strongly bound to carbon substrate probably by chemisorption. These carbonaceous intermediates do not leave the surface completely even after application of high positive pulse. Hence in this case there is disproportionally large increase of Tafel slope with temperature compared to the Au on Au or Au on Pt.

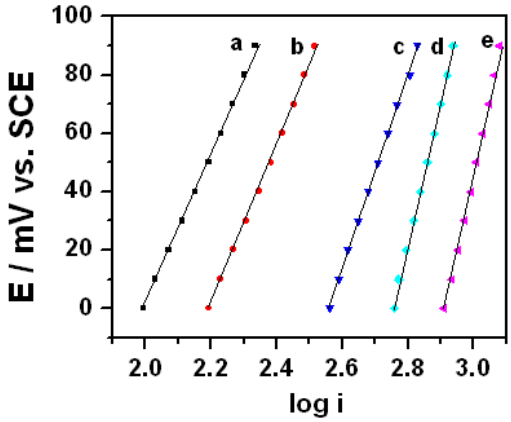

Figure 26. Tafel plot for 2 M methanol oxidation reactions of Au/C in 0.5 M NaOH, with potential programming at (a) 15 ^{0}C, (b) 20 ^{0}C, (c) 25 ^{0}C, (d) 30 ^{0}C, and (e) 35 ^{0}C.

Temperature (^{0}C)	Tafel slope (mV/dec) (with potential programming)
15	260
20	274
25	371
30	486
35	533

Table 5. Tafel slopes determined from chronoamperometry of Au on graphite for 2 M methanol oxidation reaction in 0.5 M NaOH with potential programming.

Ethanol oxidation

Chronoamperometry studies for the ethanol oxidation reactions for Au/Pt and Au/C have been carried out with and without prior potential programming. Figure 27 and Figure 28 show the Tafel plots for the ethanol oxidation reaction and Table 6 and Table 7 show the Tafel plot results. The Tafel slope increases with increase in temperature a trend observed for other systems as discussed earlier. It is also observed that the Tafel slope values are much higher in the case of ethanol oxidation than those of methanol oxidation. For example, at 25 ^{0}C the Tafel slope for ethanol on Au/Au is 277 mV compared to 228 mV for methanol on the same substrate. Again for ethanol on Au/Pt, the value is 307 mV compared to 172 mV. This shows the active sites are blocked more in the case of ethanol oxidation. This clearly means more carbonaceous intermediates block the sites in the case of ethanol oxidation. In the case of Au/C the current potential plots without prior potential programming are erratic. After application of prior

potential programming more consistent behavior was observed in this case. However, it can be seen that the Tafel slopes are 371 mV and 361 mV for methanol and ethanol which are extremely high compared to Au/Au and Au/Pt. This can be explained as due to very strong chemisorption of adsorbed intermediates on carbon surface which blocks the pores preventing the access to the Au catalyst.

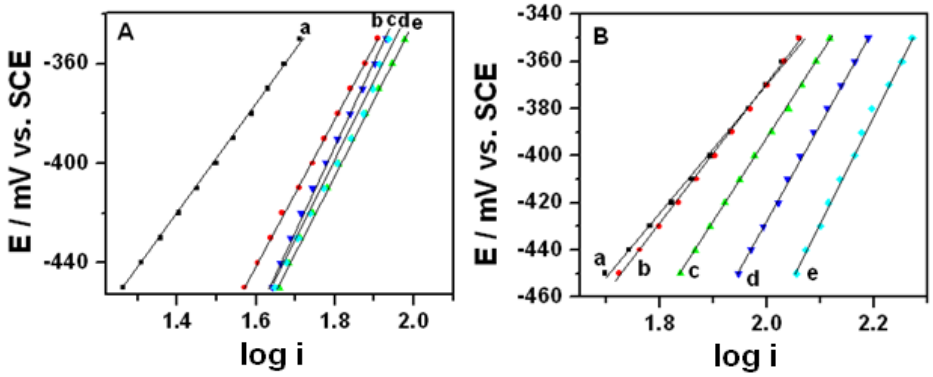

Figure 27. Tafel plots for 0.4 M ethanol oxidation reactions of Au on Pt in 0.5 M NaOH, (A) without and (B) with potential programming at (a) 15 ^{0}C, (b) 20 ^{0}C, (c) 25 ^{0}C, (d) 30 ^{0}C, and (e) 35 ^{0}C.

Temperature (^{0}C)	Tafel slope (mV/dec)	Tafel slope (mV/dec) (with potential programming)
15	221	275
20	294	296
25	307	351
30	335	412
35	330	460

Table 6. Tafel slopes determined from chronoamperometry of Au/Pt for 0.4 M ethanol oxidation reaction in 0.5 M NaOH without and with potential programming.

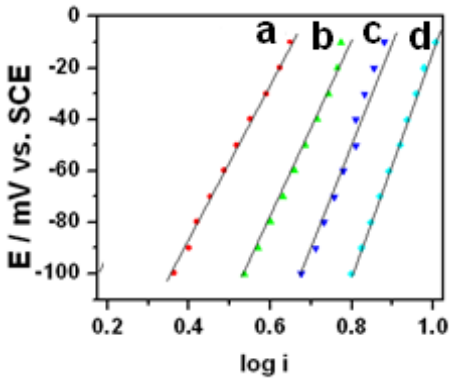

Figure 28. Tafel plots for 0.4 M ethanol oxidation reactions of Au/C in 0.5 M NaOH, (A) without and (B) with potential programming at (a) 20 ^{0}C, (b) 25 ^{0}C, (c) 30 ^{0}C, and (d) 35 ^{0}C.

Temperature (^{0}C)	Tafel slope (mV/dec) (with potential programming)
20	308
25	364
30	460
35	440

Table 7. Tafel slopes determined from CA of Au/C for 0.4 M ethanol oxidation reaction in 0.5 M NaOH with potential programming.

4.3.4 Comparison of the open circuit, onset and peak potentials on Au/Au, Au/Pt and Au/C

Table 8 and Table 9 provide a comparison of the three different electrode systems used in this work for methanol and ethanol oxidation reactions respectively. It can be seen that the open circuit potentials are higher in ethanol medium. The overpotential to be applied from the open circuit potential to reach the onset potential is quite comparable in the case of Au/Pt and Au/C for methanol and ethanol oxidation reactions (about 250 mV). It is much higher in the case of Au/Au (about 450 mV). The overpotential to reach the peak potential from OCP is more positive by 100 mV for ethanol than methanol oxidation reaction. It may also be noted that the peak potential in the case of Au/Pt occurs at relatively negative potentials corresponding to the first peak in the CV.

Electrode	OCP (mV vs SCE)	Onset potential (mV vs SCE)	Peak potential (mV vs SCE)
Au/Au	-400	40	+ 175
Au/Pt	-605	-450	-130
Au/C	-222	40	280

Table 8. Comparison of results of Au/Au, Au/Pt, and Au/C electrodes for methanol oxidation

Electrode	OCP (mV vs SCE)	Onset potential (mV vs SCE)	Peak potential (mV vs SCE)
Au/Au	-468	0	+ 175
Au/Pt	-702	-450	-150
Au/C	-353	-100	280

Table 8. Comparison of results of Au/Au, Au/Pt, and Au/C electrodes for ethanol oxidation

4.4 Conclusions

In this chapter, we have discussed the deposition of gold on gold, platinum, and graphite surfaces. The gold deposited on the Pt and graphite have been characterized using SEM, CV, and XRD. The deposited gold shows very high surface area as confirmed by CV measurements. We have studied the methanol and ethanol oxidation reactions on high real surface area gold deposited on different substrates in alkaline medium. The methanol and ethanol electro-oxidation reactions were carried out using CV and CA. CA was carried out with and without prior potential programming. Employing this methodolgy helps in estimating the influence of adsorbed intermediates formed during the electro-oxidation process on the overall kinetics of the reaction. From the CV results at different temperatures, the activation energies have been calculated for alcohol oxidation reactions. The Tafel slope were determined from the CA results at different temperatures. Tafel slope also increases with increasing temperature, which again indicates the formation of higher concentration of intermediates adsorbing onto the surface. Higher currents are obtained when potential programming was used in CA. The higher currents are due to the oxidation/desorption of adsorbed intermediates upon potential programming in CA, which provide fresh surface for each CA measurements. The potential progamming increases the slope, which is due to the higher concentration of intermediates formed due to increased reaction rate. It was also found that while on Au on Au and Au on Pt the adsorption of intermediates is rather weak, the same is not the case with Au on graphite. Here the carbonaceous intermediates chemisorb quite strongly and can not be easily removed by positive potential pulse or higher temperature or by washing the electrode sample. This is subject of more studies since the question of adsorption of carbonaceous intermediates on carbon supports used in DMFCs has not been addressed adequately in literature. Further work in this direction will reveal the realative effect of intermediate adsorption on catalyst materials (e.g Pt in DMFCs) and carbon supports.

4.5 References

[1] A. S. Arico, S. Srinivasan, V. Antonucci, *Fuel Cells* **2001**, *1*, 133.

[2] K. Jambunathan, S. Jayaraman, A. C. Hillier, *Langmuir* **2004**, *20*, 1856.

[3] K. Scott, W. M. Taama, P. Argyropoulos, *J. Power Sources* **1999**, *79*, 43.

[4] S. Park, Y. Xie, M. J. Weaver, *Langmuir* **2002**, *18*, 5792.

[5] K. J. Klabunde, R. S. Mulukutla, *Nanoscale materials in Chemsitry, John Wiley and sons, Inc., Newyork,* **2001**, 223.

[6] K. A. Assiongbon, D. Roy, *Surf. Sci.* **2005**, *594*, 99.

[7] B. Beden, C. Lamy, A. Bewick, *J. Electroanal. Chem.* **1981**, *121*, 343.

[8] S. Patra, N. Munichandraiah, *Langmuir*, **2009**, *25*, 1732.

[9] B. Viswanath, S. Patra, N. Munichandraiah, N. Ravishankar, *Langmuir*, **2009**, *25,* 3115.

[10] G. Selvarani, S. Maheswari, P. Sridhar, S. Pitchumani, A. K. Shukla, *J. Electrochem. Soc.,* **2009**, *156*, B1354.

[11] D. Zhao, B. Q. Xu, *Phys. Chem. Chem. Phys.* **2006**, *8*, 5106.

[12] D. Zhao, B.-Q. Xu, *Angew. Chem. Int. Ed.* **2006**, *45*, 4955.

[13] K. Kunimatsu, *J. Electroanal. Chem.* **1986**, *213*, 149.

[14] M. W. Breiter, *J. Electroanal. Chem.* **1967**, *14*, 407.

[15] T. Biegler, *J. Phys. Chem.* **1968**, *72*, 1571.

[16] Y. Vassilyev, V. S. Bagotsky, *Elektrokhimiya* **1975**, *11*, 1505.

[17] N. Lopez, J. K. Norskov, *J. Am. Chem. Soc.* **2002,** *124,* 11262.

[18] N. Lopez, T. V. W. Janssens, B. S. Clausen, Y. Xu, M. Mavrikakis, T. Bligaard, J. K. Norskov, *J. Catal.* **2004,** *223,* 232.

[19] C. J. Murphy, *Science* **2002**, *298*, 2139.

[20] T. S. Kim, J. D. Stiehl, C. T. Reeves, R. J. Meyer, C. B. Mullins, *J. Am. Chem. Soc.* **2003**, *125*, 2018.

[21] T. Mallat, A. Baiker, *Chem. Rev.* **2004,** *104,* 3037.

[22] H. Tsunoyama, H. Sakurai. T. Tsukuda, *Chem. Phys. Let.* **2006**, *429*, 528.

[23] C. Yu, F. Jia, Z. Ai, L. Zhang, *Chem. Mater.* **2007**, *19*, 6065.

[24] Z. Borkowska, A. Tymosiak-Zielinska, R. Nowakowski, *Electrochim. Acta* **2004**, *49*, 2613.

[25] I.-S. Park, K.-S. Lee, D.-S. Jung, H.-Y. Park, Y.-E. Sung, *Electrochim. Acta* **2007**, *52*, 5599.

[26] G. S. Attard, S. A. A. Leclerc, S. Maniguet, A. E. Russell, I. Nandhakumar, P. N. Bartlett, *Chem. Mater.* **2001**, *13*, 1444.

[27] H.-P. Liang, H.-M. Zhang, J.-S. Hu, Y.-G. Guo, L.-J. Wan, C.-L. Bai, *Angew. Chem., Int. Ed.* **2004**, *43*, 1540.

[28] X. W. Teng, X. Y. Liang, S. Rahman, H. Yang, *Ad*V. *Mater.* **2005**, *17*, 2237.

[29] B. Viswanath, N. Ravishankar, *Nanotechnology* **2007**, *18*, 475604.

[30] J. Weissmuller, R. N. Viswanath, D. Kramer, P. Zimmer, R. Wurschum, H. Gleiter, *Science* **2003**, *300*, 312.

[31] J. Jiang, T. D. Hall, L. Tsagalas, D. A. Hill, A. E. Miller, *J. Power Sources* **2006**, *162*, 977.

[32] O. T. M. Musthafa, S. Sampath, *Chem. Commun.* **2007**, *1*, 67.

[33] R. M. Rioux, H. Song, J. D. Hoefelmeyer, P. Yang, G. A. Somorjai, *J. Phys. Chem. B* **2005**, *109*, 2192.

[34] C. W. Xu, H. Wang, P. K. Shen, S. P. Jiang, *Adv. Mater.* **2007**, *19*, 4256.

[35] G. Shuyan, Z. Hongjie, W. Xiaomei, Y. Jianhui, Z. Liang, P. Chunyun, S. Dehui, M. Li, *Nanotechnology* **2005**, *16*, 2530.

[36] X. S. Peng, K. Koczkur, S. Nigro, A. C. Chen, *Chem. Commun.* **2004**, 2872.

[37] J. Weissmuller, R. N. Viswanath, D. Kramer, P. Zimmer, R. Wurschum, H. Gleiter, *Science* **2003**, *300*, 312.

[38] J. Rosler, D. Mukherji, *Adv. Eng. Mater.* **2003**, *5*, 916.

[39] M. B. Cortie, M. B. Maaroof, G. B. Smith, *Gold Bull.* **2005**, *38*, 14.

[40] J. Erlebacher, M. J. Aziz, A. Karma, N. Dimitrov, K. Sieradzki, *Nature* **2001**, *410*, 450.

[41] N. J. Robertson, H. A. Kostalik IV, T. J. Clark, P. F. Mutolo, H. D. Abruna, G. W. Coates, *J. Am. Chem. Soc.,* **2010**, *132*, 3400.

[42] S. Lu, J. Pan, A. Huang, L. Zhuang, J. Lu, **PNAS**, doi/10.1073

[43] Z. Borkowska, A. Tymosiak-Zielinska, G. Shul, *Electrochim. Acta* **2004**, *49*, 1209.

[44] J. Luo, P. N. Njoki, Y. Lan, D. Mott, L. Wang, C. J. Zhong, *Langmuir* **2006**, *22*, 2892.

[45] J. Hernandez, J. Solla-Gullon, E. Herrero, A. Aldaz, J. M. Feliu, *Electrochim. Acta* **2006**, *52*, 1662.

[46] B. K. Jena, C. Retna Raj, *Langmuir* **2007**, *23*, 4064.

[47] Y. S. Hu, Y. G. Guo, W. Sigle, S. Hore, P. Balaya, J. Maier, *Nat. Mater.* **2006**, *5*, 713.

[48] N. M. Markovic, C. A. Lucas, V. Climent, V. Stamenkovic, P. N. Ross, *Surf. Sci.* **2000**, *465*, 103.

[49] C. Jia, H. Yin, H. Ma, R. Wang, X. Ge, A. Zhou, X. Xu, Y. Ding, *J. Phys. Chem. C* **2009,** *113,* 16138.

[50] V. S. Entina, O. A. Petrii, *Electrochimiya* **1968,** *4,* 678.

[51] V. Lakshminarayanan, S. Sotiropoulos, *J. Electrochem. Soc. India* **1997,** *46-4,* 201.

[52] L. Li, Y. Xing, *Energies* **2009**, *2*, 789.

[53] R. B. de Lima, H. Varela, *Gold Bull.* **2008**, *41*, 15.

[54] G. Tremiliosi-Filho, E. R. Gonzalez, A. J. Motheo, E. M. Belgsir, J. M. Leger, C. Lamy, *J. Electroanal. Chem.* **1998**, *444*, 31.

[55] P. Ferrin, A. U. Nilekar, J. Greeley, and J. Rossmeisl, *Surf. Sci.* **2008**, *602*, 3424.

[56] N. M. Markovic, P. N. Ross, *Surf. Sci. Rep.* **2002**, *45*, 121.

[57] F. Maillard, G.-Q. Lu, A. Wieckowski, U. Stimming, *J. Phys. Chem. B* **2005**, *109*, 16230.

[58] R. Bashyam, P. Zelenay, *Nature* **2006**, *443*, 63.

[59] J. Knudsen, A. U. Nilekar, R. T. Vang, J. Schnadt, E. L. Kunkes, J. A. Dumesic, M. Mavrikakis, F. Besenbacher, *J. Am. Chem. Soc.* **2007**, *129*, 6485.

[60] J. Zhang, M. B. Vukmirovic, Y. Xu, M. Mavrikakis, R. R. Adzic, *Angew. Chem. Int. Ed.* **2005**, *44*, 2132.

[61] J. Zhang, K. Sasaki, E. Sutter, R. R. Adzic, *Science* **2007**, *315*, 220.

[62] J. Luo, P. Njoki, Y. Lin, L. Wang, D. Mott, C. J. Zhong, *Electrochem. Comm.* **2006**, *8*, 581.

[63] J. Xu, T. Zhao, Z. Liang, L. Zhu, *Chem. Mater*. **2005**, *17*, 3086.

[64] J. Luo, P. Njoki, Y. Lin, D. Mott, L. Wang, C. J. Zhong, *Langmuir* **2006**, *22*, 2892.

[65] W. H. Lizcano-Valbuena, V. A. Paganin, C. A. P. Leite, F. Galembeck, E. R. Gonzalez, *Electrochim. Acta*, **2003**, *48*, 3869.

[66] M. Carmo, V. A. Pagnin, J. M. Rosolen, E. R. Gonzalez, *J. Power Sources* **2005**, *142*, 169.